Second Harmonic Electromagnetic Emissions by an Electron Beam in Solar Wind Plasmas with Density Fluctuations

C. Krafft and P. Savoini
Laboratoire de Physique des Plasmas (LPP), CNRS, Sorbonne Université, Observatoire de Paris, Université Paris-Saclay, Ecole polytechnique, Institut Polytechnique de Paris, 91120 Palaiseau, France; catherine.krafft@universite-paris-saclay.fr

Abstract

Two-dimensional particle-in-cell simulations are performed to study the electromagnetic radiation emitted at the second harmonic $2\omega_p$ of the plasma frequency by a weak electron beam propagating in a background plasma with random density fluctuations, in solar wind conditions relevant to Type III solar radio bursts. The dynamics of the waves, the beam, and the plasma are calculated over several thousands of plasma periods. For relevant comparisons, simulations with and without applied density fluctuations are performed for the same parameters. This Letter evidences for the first time the impact of density fluctuations on the physical mechanisms driving the generation of electromagnetic waves emitted at $2\omega_p$. Results obtained show that (i) the beam radiates electromagnetic waves at $2\omega_p$ as a result of nonlinear processes of Langmuir waves' coalescence, despite wave scattering on the density fluctuations that strongly affect the Langmuir spectra; (ii) the fraction of initial beam energy transferred asymptotically to the electromagnetic waves at $2\omega_p$ is by one order of magnitude smaller when the plasma involves density fluctuations of average level around 5%; (iii) compared to the homogeneous case, the ratio of electromagnetic energy radiated at $2\omega_p$ to the energy carried by the Langmuir wave turbulence is significantly larger during all the nonlinear stage; (iv) asymptotically, when the plasma is inhomogeneous, electromagnetic emissions at $2\omega_p$ present isotropized spectra whereas quadrupolar radiation occurs for the homogeneous plasma case.

Unified Astronomy Thesaurus concepts: Solar radio emission (1522); Solar radio flares (1342); Space plasmas (1544); Plasma physics (2089)

1. Introduction

For several decades, many observations in the interplanetary space have reported that Type III solar radio bursts emit electromagnetic waves at the fundamental and the second harmonic of the electron plasma frequency ω_p (e.g., Reid & Ratcliffe 2014, and references therein). To date, several mechanisms have been proposed to explain the electromagnetic radiation emitted at the frequency $2\omega_p$. First, in the frame of the weak turbulence theory, it was argued that, whereas the nonlinear wave–wave resonant interactions between Langmuir $\mathcal{L}$ and ion sound $\mathcal{S}$ waves provide backward-propagating Langmuir waves $\mathcal{L}'$ through the electrostatic decay channel $\mathcal{L} \rightarrow \mathcal{L}' + \mathcal{S}$, the waves $\mathcal{L}$ and $\mathcal{L}'$ can merge to produce harmonic electromagnetic waves $\mathcal{H}$ at $2\omega_p$ according to the nonlinear three-waves' coalescence $\mathcal{L} + \mathcal{L}' \rightarrow \mathcal{H}$ (e.g., Melrose 1980). On another side, the so-called antenna radiation mechanism of localized Langmuir waves was also proposed (Malaspina et al. 2013), as well as processes based on the strong turbulence theory (Galeev and Krasnosel'skikh 1976), as electromagnetic radiation from intense localized Langmuir waves or solitons. More recently, some authors (Tkachenko et al. 2021) proposed a theoretical model of generation of harmonic emissions of Type III solar radio bursts in strongly inhomogeneous plasmas.

Numerical simulations performed in homogeneous plasmas have shown that second harmonic electromagnetic emissions can result from nonlinear wave–wave interactions, with correlations between the energies carried by the harmonic waves and the backward-propagating Langmuir waves (Kasaba et al. 2001; Umeda 2010). Recently, two-dimensional (2D) particle-in-cell (PIC) simulations studied the efficiency of the process leading to second harmonic emissions (Henri et al. 2019), whereas some

authors (Lee et al. 2019) solved the entire set of electromagnetic weak turbulence equations in the presence of a beam and compared these results with PIC simulations.

On another side, calculations show that density gradients in plasmas can affect the mode conversion efficiency of waves (Willes et al. 1996). Linear conversion was shown to be an efficient process to produce electromagnetic emissions at ω_p as well as backward-propagating Langmuir waves necessary for the generation of $2\omega_p$ emissions (Yin et al. 1998). More recently, it was shown using a 2D-PIC code (Sakai et al. 2005) that the process of linear conversion in a plasma with a density gradient was responsible for emission of electromagnetic waves at ω_p and $2\omega_p$.

This Letter presents 2D PIC simulations aimed at studying the second harmonic electromagnetic emissions resulting from the Langmuir wave turbulence emitted by a weak electron beam propagating in a plasma with random density fluctuations (Celnikier et al. 1983; Krupar et al. 2018). For relevant comparisons, simulations with and without applied density fluctuations are performed at the same conditions. The set of physical parameters is chosen as close as possible to solar wind conditions relevant to Type III solar radio bursts. In particular, as described below, we consider a weak and energetic beam propagating in a randomly inhomogeneous plasma with density fluctuations of average levels around a few percents of the background plasma density and wavelengths much larger than the Langmuir waves' ones (see also Krafft et al. 2013, 2015; Krafft & Volokitin 2020; Volokitin & Krafft 2020). The chosen numerical parameters provide a high grid resolution associated to a very low numerical noise and an accurate energy conservation. At this stage, it is important to point out that the background plasma density fluctuations are applied initially

and evolve self-consistently over time. The waves', the beam's, and the plasma's dynamics are calculated over several thousands of plasma periods. The objective is to evidence for the first time the physical mechanisms driving the generation, in a randomly inhomogeneous plasma with Langmuir wave turbulence, of electromagnetic emissions at the frequency $2\omega_p$, as well as the role played by the density fluctuations.

2. Model and Parameters

The simulations are performed with the open source relativistic full PIC code SMILEI (Derouillat et al. 2018), which includes both electrons and ions as finite-size particles. It solves the Maxwell and Poisson equations using a Yee mesh with centered electric and magnetic fields following the finite-difference time-domain method. The 2D3V version of SMILEI is used, which involves two spatial dimensions and three velocity components. Three species are taken into account: the background plasma's electrons and ions, as well as the beam electrons, with a realistic mass ratio $m_p/m_e = 1836$, where m_p and m_e are the proton and the electron masses.

Initially, the electron and ion plasma velocity distribution functions are Maxwellian; note that a small velocity $v_e = -n_b v_b/(n_0 - n_b)$ is applied at this stage to the background electron population (of density $n_0 - n_b$), to keep a net zero current. The beam, which propagates along the x-axis, is described by a Maxwellian drifting with the velocity v_b; its density $n_b = 5\ 10^{-4}\ n_0$ is chosen as small as possible in order to fit at most the characteristics of actual electron beams in the solar wind. In order to avoid ion acoustic wave damping, the ratio of the ion to the electron plasma temperatures is chosen as $T_i/T_e = 0.1$.

The background plasma is initiated without or with random density fluctuations δn of average level $\Delta N = \langle(\delta n/n_0)^2\rangle^{1/2} = 0.05$ and wavelengths much larger than the Langmuir waves' ones. The simulations are performed using a 2D (Cartesian geometry) grid of $N_x \times N_y = 1024 \times 1024$ cells of sizes $\Delta x = \Delta y = \sqrt{2}\ \lambda_D$, where λ_D is the electron Debye length. Then the size of the simulation plane is equal to $L_x \times L_y = 1448 \times 1448\lambda_D^2$. The normalized wavenumber resolution of the box is $\delta k_{x,y}\lambda_D = 0.0043$ (along each direction), to compare with the theoretical wavevectors' moduli of the electromagnetic waves emitted at frequency $2\omega_p$, i.e., $k\lambda_D = \sqrt{3}\ v_T/c \simeq 0.048$. The time step has been chosen in order to verify the CFL condition of the SMILEI code (Derouillat et al. 2018).

The physical parameters used are typical of Type III solar radio bursts regions in weakly magnetized solar wind and coronal plasmas. The beam drift velocity is $v_b = 9v_T$ (v_T is the thermal velocity of the background plasma), and its thermal velocity satisfies $v_{T_b} = v_T = 0.028c$, so that $v_b = 0.25c$. Long numerical computations of several thousands of plasma periods (up to $\omega_p t \simeq 8100$) are necessary to follow the full dynamics of such weak beams and the subsequent generation of electromagnetic wave emissions. The simulations are monitored by controlling the relative variation of the total energy, which is actually less than 2×10^{-4} over roughly 10^6 time steps. Note that the chosen parameters allow to keep the turbulence parameter roughly below 10^{-2} so that ponderomotive effects are not effective.

Performing PIC simulations with all these physical and numerical constraints is a challenging task. Indeed, we use 1800 particles per cell per each of the three populations (i.e., for the plasma electrons and ions as well as for the electron
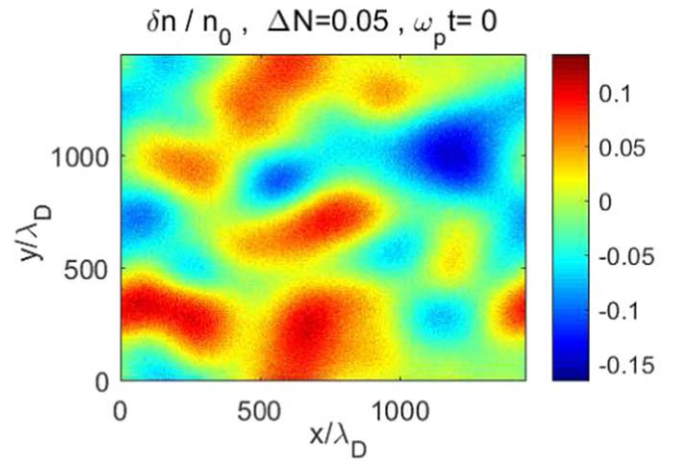

Figure 1. Initial distribution of the background plasma density fluctuations $\delta n/n_0$ in the plane (x,y), corresponding to an average level $\Delta N = \langle(\delta n/n_0)^2\rangle^{1/2} = 0.05$. The size of the box in each direction is $1448\lambda_D$.

beam). Then, the numerical noise is reduced below 10^{-2} during all the simulation time, which is much smaller than the average level $\Delta N = \langle(\delta n/n_0)^2\rangle^{1/2} = 0.05$ of the initially applied background density fluctuations and than the maximum values reached locally by $|\delta n/n_0|$ in some space regions, as one can see in Figure 1, which shows the initial spatial distribution of the density fluctuations. It is generated by inverse Fourier transform of a 2D Gaussian spectrum $\delta n_k(k_x, k_y)$ with random phases.

3. Electromagnetic Emissions

Numerical calculations are performed with the same physical and numerical parameters for both homogeneous and randomly inhomogeneous plasmas, in order to study the impact of the background fluctuations on the physical processes responsible for the electromagnetic wave radiation at frequency $2\omega_p$. Hereafter the time is normalized by the electron plasma frequency ω_p, the space coordinate by the electron Debye length λ_D, the velocity by the plasma electron thermal velocity v_T and the electric and magnetic fields E and B as $eE/(m_e c\omega_p)$ and $eB/(m_e\omega_p)$, respectively, where e is the electron charge. Two- and three-dimensional fast Fourier transforms are used, combined with Hanning windowing when necessary, and filtering using Butterworth bandpass filters. Then, the component k_x (along the x-axis) of the wavevector $\mathbf{k}$ is parallel to the direction of the electron beam propagation whereas the component k_y is perpendicular to it.

Figures 2(a)–(b) show the spatial distributions of the magnetic field component $B_z(x, y)$ at asymptotic times, when (a) the plasma is homogeneous (i.e., $\delta n(x, y) = 0$ and $\Delta N = 0$) and (b) when it is initially randomly inhomogeneous, with $\Delta N = 0.05$. Note that for $\Delta N = 0$ the length of the simulation is larger than for $\Delta N = 0.05$, as the beam relaxation process is longer. In both cases, one can observe the formation of waves propagating obliquely, with wavelengths λ_x of the order of $200\lambda_D$. Such value is in good agreement with the theoretical estimation of $k_\mathcal{H}\lambda_D \simeq 0.048$ (i.e., $\lambda_{\mathcal{H}x} \simeq 185\lambda_D$), where $\mathbf{k}_\mathcal{H}$ is the wavevector of the electromagnetic waves $\mathcal{H}$ emitted at $2\omega_p$ as a result of the coalescence $\mathcal{L} + \mathcal{L}' \rightarrow \mathcal{H}$ of the beam-driven $\mathcal{L}$ and backscattered $\mathcal{L}'$ Langmuir waves. One can observe that the density fluctuations and the subsequent waves' scattering and transformation phenomena on the inhomogeneities do not suppress but only moderately attenuate (by a factor around 2)
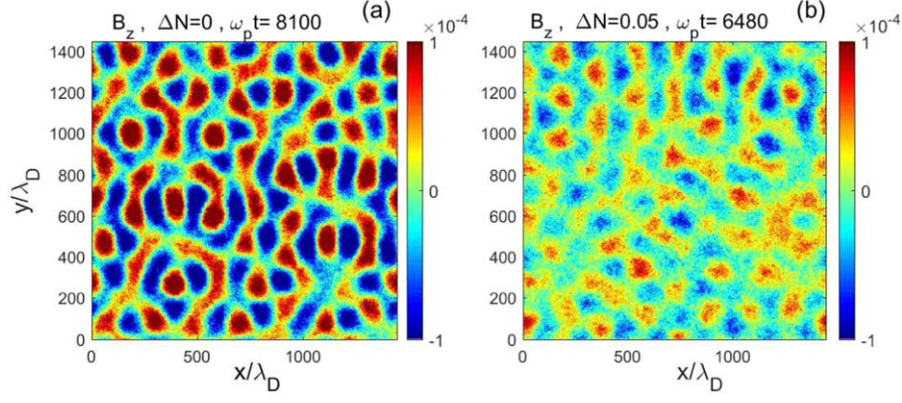
Figure 2. Isocontours of the $B_z(x, y)$ magnetic component at asymptotic times. Panel (a): the plasma is homogeneous (i.e., $\delta n(x, y) = 0$ and $\Delta N = 0$) and the asymptotic time is $\omega_p t = 8100$. Panel (b): the plasma is initially randomly inhomogeneous, with $\Delta N = 0.05$; the asymptotic time is $\omega_p t = 6480$.
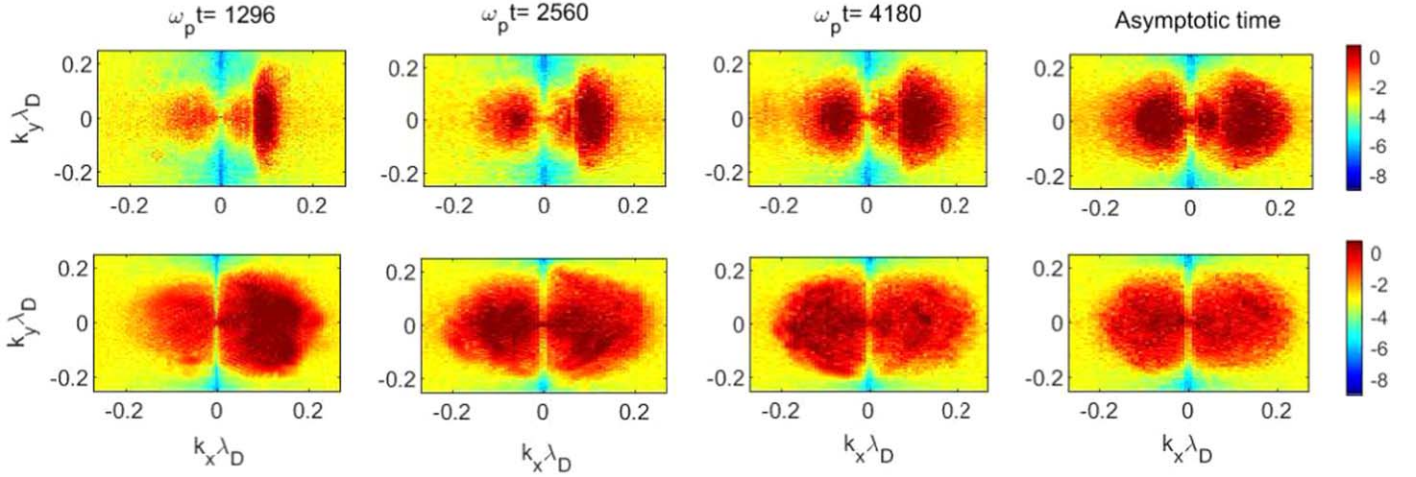

Figure 3. Distributions in the (k_x, k_y)-space of the normalized electric wave spectral energy density $\log_{10}|E_{xk}|^2$ emitted at the frequency $\omega_k \simeq \omega_p$, for $\Delta N = 0$ (top row) and $\Delta N = 0.05$ (bottom row). The first three columns correspond to the times $\omega_p t = 1296$, $\omega_p t = 2560$ and $\omega_p t = 4180$; the last column shows the spectra near asymptotic times, i.e., at $\omega_p t = 7960$ for $\Delta N = 0$ and at $\omega_p t = 6350$ for $\Delta N = 0.05$.

the amplitudes of the electromagnetic emissions. Note that the presence of density fluctuations modifies the resonance conditions whether it is (i) between the beam electrons and the primary Langmuir waves $\mathcal{L}$, or (ii) between the beam-driven and the backscattered Langmuir waves $\mathcal{L}$ and $\mathcal{L}'$ during their nonlinear interactions. Mechanisms as wave refraction, reflection, conversion, tunneling, trapping, localization, or/and diffusion lead to the transport of wave energy toward smaller or larger wavevector scales, depending on the characteristics (average level, wavelengths, variability, etc.) of the random density fluctuations, and eventually modify strongly the Langmuir wave spectra, as shown hereafter.

Figure 3 shows at different times during the saturation stage of the beam instability (i.e., at $\omega_p t \gtrsim 1000$), the distributions in the (k_x, k_y)-space of the electric wave spectral energy densities $|E_{xk}|^2$ (in logarithmic scale) emitted at the frequency $\omega_k \simeq \omega_p$, for $\Delta N = 0$ (top row) and $\Delta N = 0.05$ (bottom row), where $E_{xk}(k_x, k_y)$ is the Fourier transform of the electric field $E_x(x, y)$. One can observe the excitation of Langmuir waves $\mathcal{L}$ (around $k_{\mathcal{L}x} \lambda_D \simeq 0.1$) and $\mathcal{L}'$ (around $k_{\mathcal{L}'x} \lambda_D \simeq -0.07$); $\mathbf{k}_{\mathcal{L}}$ and $\mathbf{k}_{\mathcal{L}}$ are the wavevectors of the waves $\mathcal{L}$ and $\mathcal{L}'$. For $\Delta N = 0$, the spectra widen significantly when time increases, along the x and y directions, due to the beam relaxation process and the subsequent energy transfer to larger wavenumbers. Such observations are in good agreement with calculations performed in the frame of the electromagnetic weak

turbulence theory (Ziebell et al. 2015). The backscattered waves $\mathcal{L}'$ mainly result from the electrostatic three-waves' decay $\mathcal{L} \rightarrow \mathcal{L}' + \mathcal{S}$, where $\mathcal{S}$ are ion acoustic waves with $k_{\mathcal{S}x} \simeq 2k_{\mathcal{L}x}$ (see forthcoming paper). Meanwhile, for $\Delta N = 0.05$ (Figure 3, bottom row), the spectral broadening occurs earlier and more strongly, even before wave saturation is reached, as the linear scattering phenomena of the Langmuir waves $\mathcal{L}$ on the density fluctuations transform them, notably into backward-propagating Langmuir waves with $k_x < 0$. Thus, if in both cases $\Delta N = 0$ and $\Delta N = 0.05$ one observes that energy is transferred as time increases from the Langmuir waves $\mathcal{L}$ with positive $k_x > 0$ to those with negative $k_x < 0$, it is likely not owing to the same process, even if for $\Delta N = 0.05$, the Langmuir waves $\mathcal{L}$ also experience electrostatic decay. Asymptotically, energy is approximately equivalently shared between positive and negative $\mathbf{k}$-space regions, for both directions x and y.

Let us now examine in Figure 4 the corresponding logarithmic distributions of the magnetic wave spectral energy density $|B_{zk}|^2$ emitted at the harmonic frequency $\omega_k \simeq 2\omega_p$, for $\Delta N = 0$ (top row) and $\Delta N = 0.05$ (bottom row), for the same times as in Figure 3; $B_{zk}(k_x, k_y)$ is the Fourier transform of the magnetic field component $B_z(x, y)$. For the homogeneous plasma case (top row), one observes that, as time increases starting from $\omega_p t = 1296$, the circular structure of radius $k\lambda_D \simeq \sqrt{3}\, v_T/c$, which corresponds to
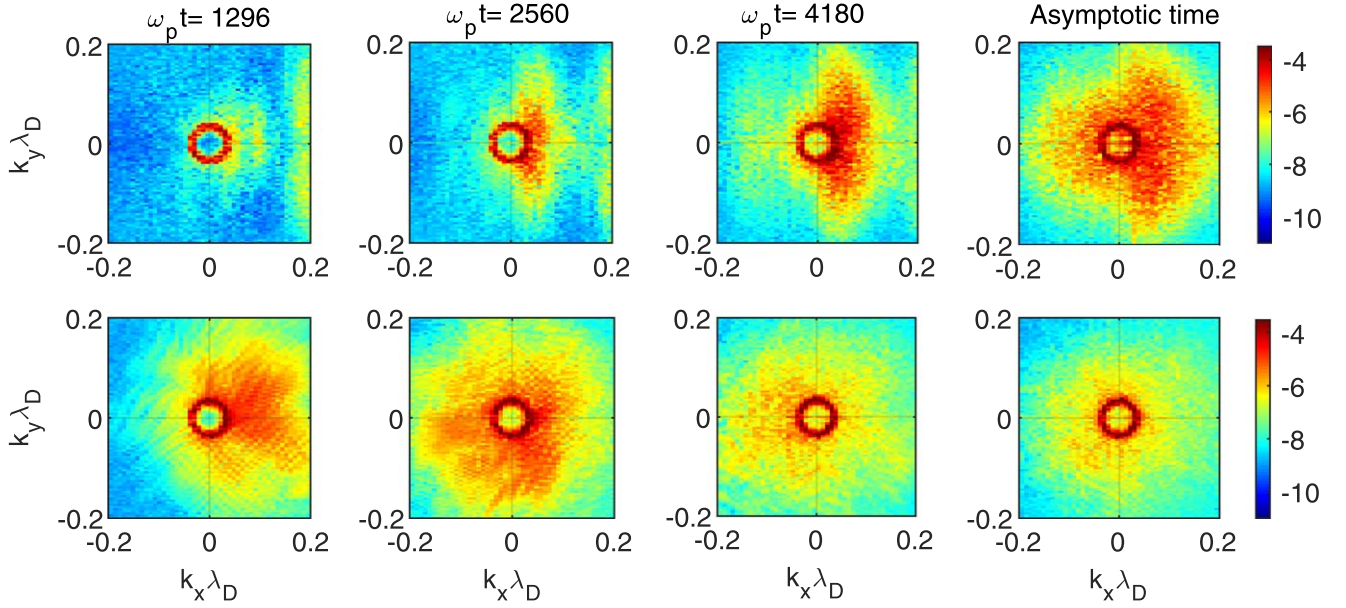
Figure 4. Distributions of the normalized magnetic wave spectral energy densities $\log_{10}(|B_{zk}|^2)$ emitted at the harmonic frequency $\omega_k \simeq 2\omega_p$, for $\Delta N = 0$ (top row) and $\Delta N = 0.05$ (bottom row). The times of each column are the same as in Figure 3.

the dispersion of transverse waves at frequency $\omega_k \simeq 2\omega_p$, begins to diffuse toward positive k_x, presenting asymptotically the quadrupolar-type emission predicted by the theory (Melrose 1980). At the same time $\omega_p t = 1296$ but for $\Delta N = 0.05$ (bottom row), one can note the presence of electromagnetic waves at $\omega_k \simeq 2\omega_p$ (circle), together with magnetic energy diffusing slightly toward $k_x > 0$, in agreement with the occurrence of the coalescence process $\mathcal{L} + \mathcal{L}' \rightarrow \mathcal{H}$ whose resonant conditions impose that $k_{\mathcal{H}x} = k_{\mathcal{L}x} + k_{\mathcal{L}'x} = k_{\mathcal{L}x} - |k_{\mathcal{L}'x}|$; it follows that $k_{\mathcal{H}x}$ should be mostly positive, because at the early time considered ($\omega_p t = 1296$), there is more electric energy $|E_{xk}|^2$ carried by waves $\mathcal{L}$ with $k_{\mathcal{L}x} > |k_{\mathcal{L}'x}|$ than by waves $\mathcal{L}'$ with $|k_{\mathcal{L}'x}| > k_{\mathcal{L}x}$ (see Figure 3). At the next time $\omega_p t = 2560$, the energy density $|E_{xk}|^2$ is almost equivalently shared between the primary and the back-scattered Langmuir waves (Figure 3, bottom row), as it can also be observed for the magnetic energy density distribution $|B_{zk}|^2$ at the same time, diffused in both half planes $k_x > 0$ and $k_x < 0$. The significant anisotropy between $k_{\mathcal{H}y} < 0$ and $k_{\mathcal{H}y} > 0$ is also visible in the beam-driven Langmuir waves' spectrum (Figure 3, bottom row). Further, at $\omega_p t = 4180$, the same conclusions can be stated; the magnetic energy density is more concentrated in the half plane where $k_{\mathcal{H}x} < 0$, in agreement with the fact that more energy is carried by waves $\mathcal{L}'$ with $|k_{\mathcal{L}'x}| > k_{\mathcal{L}x}$ than by waves $\mathcal{L}$ with $k_{\mathcal{L}x} > |k_{\mathcal{L}'x}|$. The picture presented at the asymptotic time confirms these observations: the magnetic field spectrum tends to be isotropized, as it is also the case for the energy distribution of the asymptotic Langmuir spectrum, contrary to the homogeneous plasma case where quadrupolar emission occurs. All these findings, which can also be partly applied to the case $\Delta N = 0$, tend to confirm that the observed electromagnetic waves emitted at $2\omega_p$ result from the coalescence $\mathcal{L} + \mathcal{L}' \rightarrow \mathcal{H}$, for both values of ΔN. The following pictures will bring additional arguments in this favor.

The first column of Figure 5 shows, for the homogeneous plasma ($\Delta N = 0$, top row (panel (a)) and the plasma with density fluctuations ($\Delta N = 0.05$, bottom row (panel (c)), the variations with time of the energies $W_{\mathcal{L}} \simeq (1/2) \iint |E_{\mathcal{L}x}|^2 dxdy$ and $W_{\mathcal{L}'} \simeq (1/2) \iint |E_{\mathcal{L}'x}|^2 dxdy$ carried by the Langmuir waves

$\mathcal{L}$ and $\mathcal{L}'$ at frequency $\omega_k \simeq \omega_p$, as well as the energy $W_{\mathcal{H}} \simeq (1/2) \iint |B_{\mathcal{H}z}|^2 dxdy$ of the electromagnetic waves $\mathcal{H}$ at frequency $\omega_k \simeq 2\omega_p$; $E_{\mathcal{L}x}$, $E_{\mathcal{L}'x}$, and $B_{\mathcal{H}z}$ are the electric and magnetic fields associated with the waves $\mathcal{L}$, $\mathcal{L}'$, and $\mathcal{H}$, respectively. These values have been obtained by selecting the adequate frequencies' and wavevectors' domains corresponding to the waves' characteristics when performing the sums $\sum_{k_x,k_y,\omega_k} |E_{xk}(\omega_k, k_x, k_y)|^2$ and $\sum_{k_x,k_y,\omega_k} |B_{zk}(\omega_k, k_x, k_y)|^2$, where $E_{xk}(\omega_k, k_x, k_y)$ and $B_{zk}(\omega_k, k_x, k_y)$ are the 3D Fourier transforms of $E_x(t, x, y)$ and $B_z(t, x, y)$. All of the energies are normalized by the initial beam kinetic energy.

For both ΔN, the energies of the waves $\mathcal{L}$ increase with a quasi-similar linear growth rate (however, this is significantly smaller for $\Delta N = 0.05$), and saturate around $\omega_p t \sim 1000$, whereas the waves $\mathcal{L}'$ and $\mathcal{H}$ grow with the same (for $\Delta N = 0.05$) or close (for $\Delta N = 0$) rates. When the plasma is inhomogeneous, the growth rate of the waves $\mathcal{L}'$ and $\mathcal{H}$ is roughly 2 times larger than for $\Delta N = 0$, and their saturation occurs a few thousands of plasma periods earlier. Indeed, beam-driven Langmuir waves' scattering on density fluctuations leads to the production of backscattered waves mainly through linear phenomena whereas, when the plasma is homogeneous, the generation of these waves results mostly from the nonlinear resonant decay $\mathcal{L} \rightarrow \mathcal{L}' + \mathcal{S}$. Asymptotically, the saturation levels reached by the waves $\mathcal{L}$ and $\mathcal{L}'$ have close values, due to efficient energy transfers from the beam-driven to the backscattered waves. In turn, the waves $\mathcal{H}$ saturate near the normalized energy levels around 10^{-4} and 10^{-5}, for $\Delta N = 0$ and $\Delta N = 0.05$, respectively. It means that asymptotically, in the homogeneous plasma, a fraction of 10^{-4} of the initial beam energy is used for the generation of the waves $\mathcal{H}$, whereas for the inhomogeneous plasma, this fraction is one order of magnitude less. This reduction is likely due to the damping of the beam-driven Langmuir waves occurring just after their saturation whereas, for the homogeneous plasma, damping appears later and with a slower rate. Figure 5(e) presents the time variation of the ratios w of $W_{\mathcal{H}}$ to the normalized energy $W_{\mathcal{L}} + W_{\mathcal{L}'}$ carried by the Langmuir turbulence, for $\Delta N = 0.05$ and $\Delta N = 0$. In the linear stage, both curves are very close but,
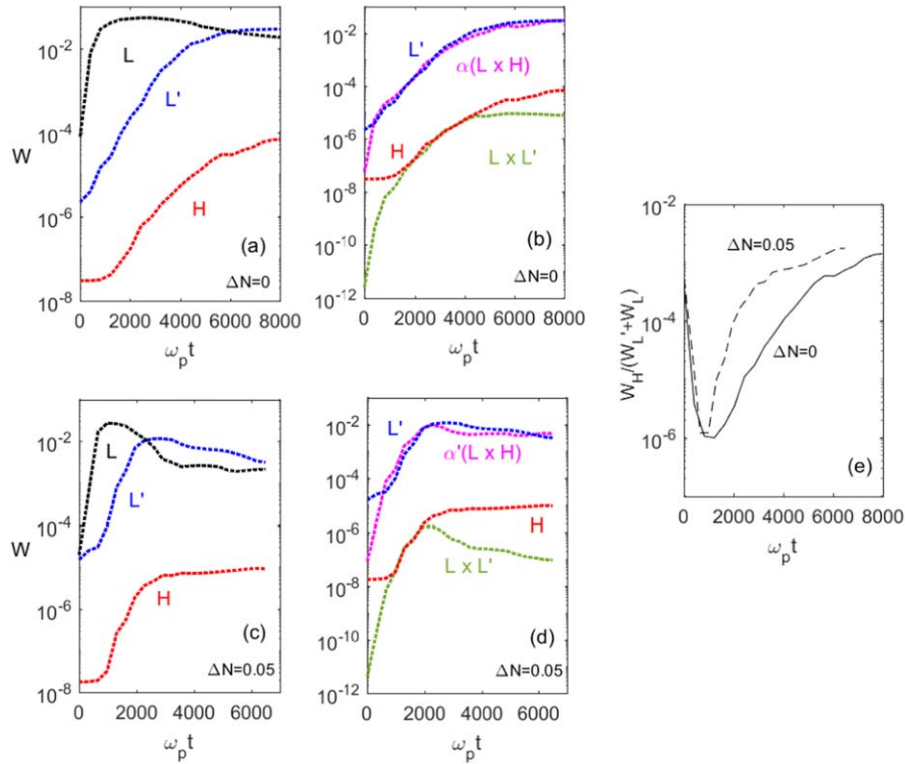
Figure 5. Panels (a–b): homogeneous plasma ($\Delta N = 0$); panels (c–d): inhomogeneous plasma with density fluctuations ($\Delta N = 0.05$). First column: variations with the time $\omega_p t$ of the energies $W_{\mathcal{L}}$ and $W_{\mathcal{L}'}$ carried by the beam-driven Langmuir waves $\mathcal{L}$ (black dotted lines labeled by "L"), by the backscattered Langmuir waves $\mathcal{L}'$ (blue dotted lines labeled by "L'") at frequency ω_p, and of the energy $W_{\mathcal{H}}$ carried by the electromagnetic waves $\mathcal{H}$ of frequency $2\omega_p$ (red dotted lines labeled by "H"). Second column: variations with $\omega_p t$ of the energy $W_{\mathcal{H}}$ (red dotted lines) and of the product $W_{\mathcal{L}} W_{\mathcal{L}'}$ (green dotted lines labeled by "$L \times L'$"), as well as of the energy $W_{\mathcal{L}'}$ (blue dotted lines) and the product $\alpha W_{\mathcal{L}} W_{\mathcal{H}}$ (pink dotted lines labeled by "$\alpha(L \times H)$" for $\Delta N = 0$ and "$\alpha'(L \times H)$" for $\Delta N = 0.05$); the multiplication by the factors α or α' allows to evidence more clearly by superimposition of the curves the close link between the red and the green curves, as well as the pink and the blue curves. Panel (e): time variation of the ratio $w = W_{\mathcal{H}}/(W_{\mathcal{L}} + W_{\mathcal{L}'})$ for $\Delta N = 0$ (solid line) and $\Delta N = 0.05$ (dashed line). The energies are normalized by the initial beam kinetic energy.

during the nonlinear saturation, the ratio w is always significantly larger for $\Delta N = 0.05$, by almost one order of magnitude, and around a factor of 2 at asymptotic times. Then we can state that the fraction of Langmuir wave turbulent energy transferred asymptotically to the electromagnetic radiation at $2\omega_p$ is significantly larger when the plasma is randomly inhomogeneous, reaching values larger than 10^{-3}.

The second column of Figure 5 ($\Delta N = 0$, top row (panel (b)) and ($\Delta N = 0.05$, bottom row (panel (d)) shows the time variations of $W_{\mathcal{H}}$ and the product $W_{\mathcal{L}} W_{\mathcal{L}'}$, as well as the time variations of $W_{\mathcal{L}'}$ and $W_{\mathcal{L}} W_{\mathcal{H}}$, multiplied by a coupling factor α (or α', depending on ΔN). One observes that, for both ΔN, the curves are perfectly superimposed or follow closely the same growth during the generation process of the waves $\mathcal{H}$, what confirms that $W_{\mathcal{H}}$ is proportional to $W_{\mathcal{L}} W_{\mathcal{L}'}$ in this time range, relation which has to be satisfied if the waves $\mathcal{L}$, $\mathcal{L}'$, and $\mathcal{H}$ interact resonantly via a three-waves nonlinear process. The coalescence $\mathcal{L} + \mathcal{L}' \rightarrow \mathcal{H}$ actually takes place. Moreover one can see that, except at the most early times, $W_{\mathcal{L}'} \propto W_{\mathcal{L}} W_{\mathcal{H}}$ during all the simulation time, with a proportionality factor α for $\Delta N = 0$ and α' for $\Delta N = 0.05$.

4. Conclusion

Two-dimensional PIC simulations are performed to study the electromagnetic radiation emitted at the second harmonic $2\omega_p$ of the plasma frequency by a weak electron beam propagating in a background plasma with random density fluctuations, in solar wind conditions relevant to Type III solar radio bursts. The dynamics of the waves, the beam and the plasma are calculated over several

thousands of plasma periods. For relevant comparisons, simulations with and without applied density fluctuations are performed for the same parameters. This Letter evidences for the first time the impact of density fluctuations on the physical mechanisms driving the generation of electromagnetic waves emitted at $2\omega_p$.

More precisely, results obtained show that: (i) the beam radiates electromagnetic waves at $2\omega_p$ as a result of nonlinear processes of Langmuir waves' coalescence, according to the channel $\mathcal{L} + \mathcal{L}' \rightarrow \mathcal{H}$, despite the presence of linear phenomena of waves' scattering and transformations on the density fluctuations that strongly affect the Langmuir wave spectra; (ii) the fraction of initial beam energy transferred asymptotically to the electromagnetic waves at $2\omega_p$, which is of the order of 10^{-4} for the homogeneous plasma, is by one order of magnitude smaller when the plasma involves density fluctuations of average level around 5%; (iii) nevertheless, compared to the homogeneous case, the ratio of electromagnetic energy radiated at frequency $2\omega_p$ to the energy carried by the Langmuir wave turbulence is significantly larger during all the nonlinear stage, reaching asymptotically values larger than 10^{-3}; moreover, the growth rate of the electromagnetic waves' generation is also larger when density fluctuations are present, as backscattered Langmuir waves $\mathcal{L}'$ are produced at early times due to linear interaction phenomena of waves with density fluctuations, so that beam-driven Langmuir waves $\mathcal{L}$ do not need to reach sufficiently large amplitudes to produce them by nonlinear decay; (iv) asymptotically, when the plasma is inhomogeneous, the electromagnetic emissions at $2\omega_p$ present isotropized spectra whereas quadrupolar radiation occurs for the homogeneous plasma case.

ORCID iDs

C. Krafft ⓘ https://orcid.org/0000-0002-8595-4772

References

Celnikier, L. M., Harvey, C. C., Jegou, R., Moricet, P., & Kemp, M. 1983, A&A, 126, 293
Derouillat, J., Beck, A., Perez, F., et al. 2018, CoPhC, 222, 351
Galeev, A., & Krasnosel'skikh, V. 1976, JETP Lett, 24, 515
Henri, P., Sgattoni, A., Briand, C., Amiranoff, F., & Riconda, C. 2019, JGRA, 124, 1475
Kasaba, Y., Matsumoto, H., & Omura, Y. 2001, JGR, 106, 18693
Krafft, C., & Volokitin, A. S. 2020, PPCF, 62, 024007
Krafft, C., Volokitin, A. S., & Krasnoselskikh, V. V. 2013, ApJ, 778, 111
Krafft, C., Volokitin, A. S., & Krasnoselskikh, V. V. 2015, ApJ, 809, 176
Krupar, V., Maksimovic, M., Kontar, E. P., et al. 2018, ApJ, 857, 82
Malaspina, D. M., Graham, D. B., Ergun, R. E., & Cairns, I. H. 2013, JGRA, 118, 6880
Melrose, D. B. 1980, SoPh, 67, 357
Reid, H. A. S., & Ratcliffe, H. 2014, RAA, 14, 773
Sakai, J. I., Kitamoto, T., & Saito, S. 2005, ApJL, 622, L157
Lee, S.-Y., Ziebell, L. F., Yoon, P. H., et al. 2019, ApJ, 871, 74
Tkachenko, A., Krasnoselskikh, V., & Voshchepynets, A. 2021, ApJ, 908, 126
Umeda, T. 2010, JGRA, 115, A01204
Volokitin, A. S., & Krafft, C. 2020, ApJL, 893, L47
Willes, A. J., Robinson, P. A., & Melrose, D. B. 1996, PhPl, 3, 149
Yin, L., Ashour-Abdalla, M., E1-Alaoui, M., Bosqued, J. M., & Bougeret, J. L. 1998, GeoRL, 25, 2609
Ziebell, L. F., Yoon, P. H., Petruzzellis, L. T., Gaelzer, R., & Pavan, J. 2015, ApJ, 806, 237